Protein Engineering, Design & Selection vol. 22 no. 3 pp. 121–134, 2009
Published online January 10, 2009 doi:10.1093/protein/gzn077

The influence of the framework core residues on the biophysical properties of immunoglobulin heavy chain variable domains

Annemarie Honegger, Alain Daniel Malebranche[1], Daniela Röthlisberger[2] and Andreas Plückthun[3]

Biochemisches Institut der Universität Zürich, Winterthurerstrasse 190, CH-8057 Zürich, Switzerland

[1]Present address: University of British Columbia, Faculty of Medicine, Class of 2011, Vancouver, BC V6T 1Z3, Canada.

[2]Present address: Department of Biochemistry, University of Washington, HSB J555, Box 357350, Seattle, WA 98195, USA.

[3]To whom correspondence should be addressed.
E-mail: plueckthun@bioc.uzh.ch

Antibody variable domains differ considerably in stability. Single-chain Fv (scFv) fragments derived from natural repertoires frequently lack the high stability needed for therapeutic application, necessitating reengineering not only to humanize their sequence, but also to improve their biophysical properties. The human V_H3 domain has been identified as having the best biophysical properties among human subtypes. However, complementarity determining region (CDR) grafts from highly divergent V_H domains to huV_H3 frequently fail to reach its superior stability. In previous experiments involving a CDR graft from a murine V_H9 domain of very poor stability to huV_H3, a hybrid V_H framework was obtained which combines the lower core residues of muV_H9 with the surface residues of huV_H3. It resulted in a scFv with far better biophysical properties than the corresponding grafts to the consensus huV_H3 framework. To better understand the origin of the superior properties of the hybrid framework, we constructed further hybrids, but now in the context of the consensus CDR-H1 and -H2 of the original human V_H3 domain. The new hybrids included elements from either murine V_H9, human V_H1 or human V_H5 domains. From guanidinium chloride-induced equilibrium denaturation measurements, kinetic denaturation experiments, measurements of heat-induced aggregation and comparison of soluble expression yield in *Escherichia coli*, we conclude that the optimal V_H framework is CDR-dependent. The present work pinpoints structural features responsible for this dependency and helps to explain why the immune system uses more than one framework with different structural subtypes in framework 1 to optimally support widely different CDRs.

Keywords: antibody engineering/framework 1 structure/immunoglobulin variable domains/scFv fragment/stability

Introduction

Antibodies differ considerably in sequence, not only within their complementarity determining regions (CDRs), but also in the framework (FR), with significant consequences for their biophysical properties. These sequence differences are encoded in the different V-genes, and can get further amplified by somatic point mutations. However, we are mostly concerned here with the conserved differences between whole germline families and the structural subtypes encoded by them.

Based on sequence homology, human V_H-genes can be clustered into seven, murine into 15 germline families (IMGT database, (Lefranc *et al*., 2005)), with only 36% sequence identity between the consensus sequences representing the most distantly related human V_H germline families, huV_H1 and huV_H2, and 31% sequence identity between the consensus sequences of the most distantly related murine V_H germline families, muV_H1 and muV_H8 [91–101 amino acids compared, residues H1–H108 according to the AHo numbering scheme used throughout this paper (Honegger and Plückthun, 2001a), corresponding to residues H1–H94 according to Kabat *et al.* (1991)]. If CDR-H1 and CDR-H2 are omitted from this analysis, the numbers increase still only to 42% identity between the most distant human and 35% identity between the most distant murine sequences (76 amino acids compared). Thus, while the germline sequences have diverged significantly within one species, one finds more closely homologous families between mouse and man: the human germline family consensus sequences show between 60% (huV_H5/muV_H14) and 81% (huV_H3/muV_H5) sequence identity to the closest murine consensus sequence, 66–84% if only the framework residues are compared.

In view of the large evolutionary distance between the different antibody germline families within the same species, it is not surprising that the biophysical properties of the proteins derived from these sequences vary considerably. Ewert *et al.* (2003) systematically compared the biophysical properties of isolated human antibody variable domains representing the consensus sequences of the different germline families and of the single-chain Fv (scFv) fragments composed of these consensus domains. huV_H3 was found to be the most stable of the human frameworks, followed by huV_H1 and huV_H5, whereas huV_H2, huV_H4 and particularly huV_H6 showed very poor biophysical properties. huV_H7 was not tested, as in the HuCAL® consensus framework design it was treated as a member of the huV_H1 family (Knappik *et al*., 2000).

The stability of different antibody constructs containing a V_H domain derived from the same germline family can vary widely, depending on the CDR-H3 sequence, germline-encoded V-sequence variability, somatic mutations, the nature of the V_L domain and the degree of mutual stabilization of interacting domains (Wörn and Plückthun, 1999). Nonetheless, huV_H3-like sequences and associated structural features of this family are highly overrepresented amongst the V_H domains of exceptionally stable antibody constructs. This was found both for antibodies of human and non-human origin, and was especially visible in disulfide-free constructs

(Proba *et al*., 1997, 1998) or in intrabodies (Marasco, 1995) selected for the stability in a reducing environment, both of which cannot rely on the stabilizing influence of the disulfide bond. Camelid V_{HH} domains, capable of functioning in the absence of a V_L domain (Hamers-Casterman *et al*., 1993; Ewert *et al*., 2002) also fall into the class of huV$_H$3-like V_H domains. Around 50% of all functional human germlines (27 out of 57 genes) belong the huV$_H$3 family, making this the largest germline family in the human repertoire. For these reasons, the huV$_H$3 consensus framework is the most frequently used human acceptor framework for CDR grafts (Jones *et al*., 1986; Eigenbrot *et al*., 1993), which are performed primarily to reduce the immunogenicity of an antibody-derived construct in therapeutic applications in humans, but as a fringe benefit may also improve their biophysical properties. Single framework libraries have also been constructed based on this type of framework (Pini *et al*., 1998; Söderlind *et al*., 2000; Röthlisberger *et al*., 2004; Fellouse *et al*., 2005; Fellouse *et al*., 2007).

From a structural standpoint, and ignoring CDR lengths and conformations, natural V_H frameworks can be grouped into three (human) or four (mouse) distinct structural subtypes (Saul and Poljak, 1993; Saul, 1994; Honegger and Plückthun, 2001b; Jung *et al*., 2001). The most striking difference between those subclasses lies in the conformation of the kink connecting strands A′ and A″ in the framework 1 region of the domain (Fig. 1A–D). This conformational difference is caused by the fully buried side chain of a glutamate or glutamine in position H6 that has to assume a different conformation depending on its identity in order to satisfy the different hydrogen bonding requirements. The glutamate side chain can only serve as a hydrogen bond acceptor (Fig. 2A), while the glutamine side chain is both a hydrogen bond acceptor and a donor (Fig. 2B), which results in hydrogen bonds to different main chain peptide NH and CO groups and to the side chain OH of Thr H143. The side-chain orientation enforced by these hydrogen bonds affects the main-chain conformation, as it does not allow the continuation of the A′ β-strand, but enforces a kink in the chain. The actual shape of the kink is further modulated by the flexibility of residues H7–H10 within the kink (Honegger and Plückthun, 2001b; Jung *et al*., 2001). Additional, more subtle, differences of the backbone conformation throughout the entire domain become apparent upon superposition of multiple structures: a slight difference in the relative orientation of the inner β-sheet (forming the heterodimer interface) and the outer β-sheet, which together form the β-sandwich structure of the immunoglobulin fold, can be noted, as well as slight differences in the take-off angle of CDR-H2 (Fig. 1E and F).

While the lower core of the V_L domains is fairly conserved across all germlines, even between lambda and kappa chains, the subtype-dependent variations in the backbone conformation of the V_H domains impose constraints on the packing of the hydrophobic residues in the core of the domain. This core packing, though highly conserved within any one of the V_H germline families, shows significant variations from one germline family to the next. Successfully grafting the complementary determining regions of an antibody to structurally divergent frameworks is only possible because the core can be divided into an upper core and a lower core (Fig. 3), bisected by a layer of highly conserved residues: the upper core consists mainly of buried CDR residues, but some additional residues from the N-terminal region and the outer loop pack against key CDR residues and usually have to be grafted along with the CDR residues in order to maintain the full antigen binding affinity. The dividing layer between upper and lower core consists mainly of the disulfide bond (Cys H23–Cys H106) and the core tryptophan (Trp H23). Glu/Gln H6, while playing a large part in the variability of the lower core does not directly affect the upper core: the conformational difference between Glu and Gln in that position consists mainly in a rotation around the long axis of the side chain that enforces a change in main-chain conformation with little change in the volume filled by the side chain (Fig. 1B). The lower core consists of the hydrophobic core residues H19, H21, H55, H56, H74, H78, H91, H93, H96, H102, H104 and H145 discussed in this paper. These residues co-vary with the antibody germline family. In addition, a cluster of charged residues (H45, H53, H77 H97, H99, H100) in the lower core of the V_H domain has been kept constant in all constructs. This clean division between upper and lower core breaks down in the area of CDR-H2. The boundaries of CDR-H2 are not clearly delineated, and buried CDR-residues pack against lower core residues that vary by subtype. In addition, the take-off angle and conformation of CDR-H2 differ between different germline families and structural subtypes. These differences are in part due to different CDR-H2 length and specific CDR-H2 sequence features, in part to the interactions between CDR-H2 and residues in the lower core.

In the design of a CDR graft for humanization and/or stabilization (Ewert *et al*., 2004) one often has to make a choice: on the one hand, a graft to the human framework most closely related to the framework of the CDR donor minimizes the probability of losing binding affinity, but may lead to a construct of equally insufficient stability as the donor. In contrast, grafting to the most stable of the human V_L and V_H frameworks reduces the risk of producing a construct with insufficient stability, but increases the risk of reducing antigen binding affinity. To further complicate matters, the most stable framework is not necessarily the one that gives the best production yields in a given expression system, as huV$_H$1 appears to be somewhat less aggregation-prone and is produced with higher yields than huV$_H$3 upon soluble periplasmic expression in *Escherichia coli* (Ewert *et al*., 2003).

The question thus arises whether there might be more appropriate acceptor frameworks for loop grafting than huV$_H$3. One such candidate has been identified from previous loop grafting experiments. The scFv Moc31 is derived from a murine monoclonal antibody with a muVκ2 light- and a muV$_H$9 heavy-chain variable domain and directed against the cell surface glycoprotein EpCAM (EGP2) (Myklebust *et al*., 1991), and it was converted to the humanized scFv 4D5MocA (Willuda *et al*., 1999) by standard CDR grafting to the huVκ1 and huV$_H$3 consensus frameworks. These domains had also been used in the humanization of antibody 4D5 (Eigenbrot *et al*., 1993). Taking into account the possibility that the framework subtype and associated core packing differences might affect the CDR-H2 take-off angle as suggested by Saul and Poljak (Saul and Poljak, 1993; Saul, 1994) and the difference in the relative orientation of the two β-sheets observed in the comparison

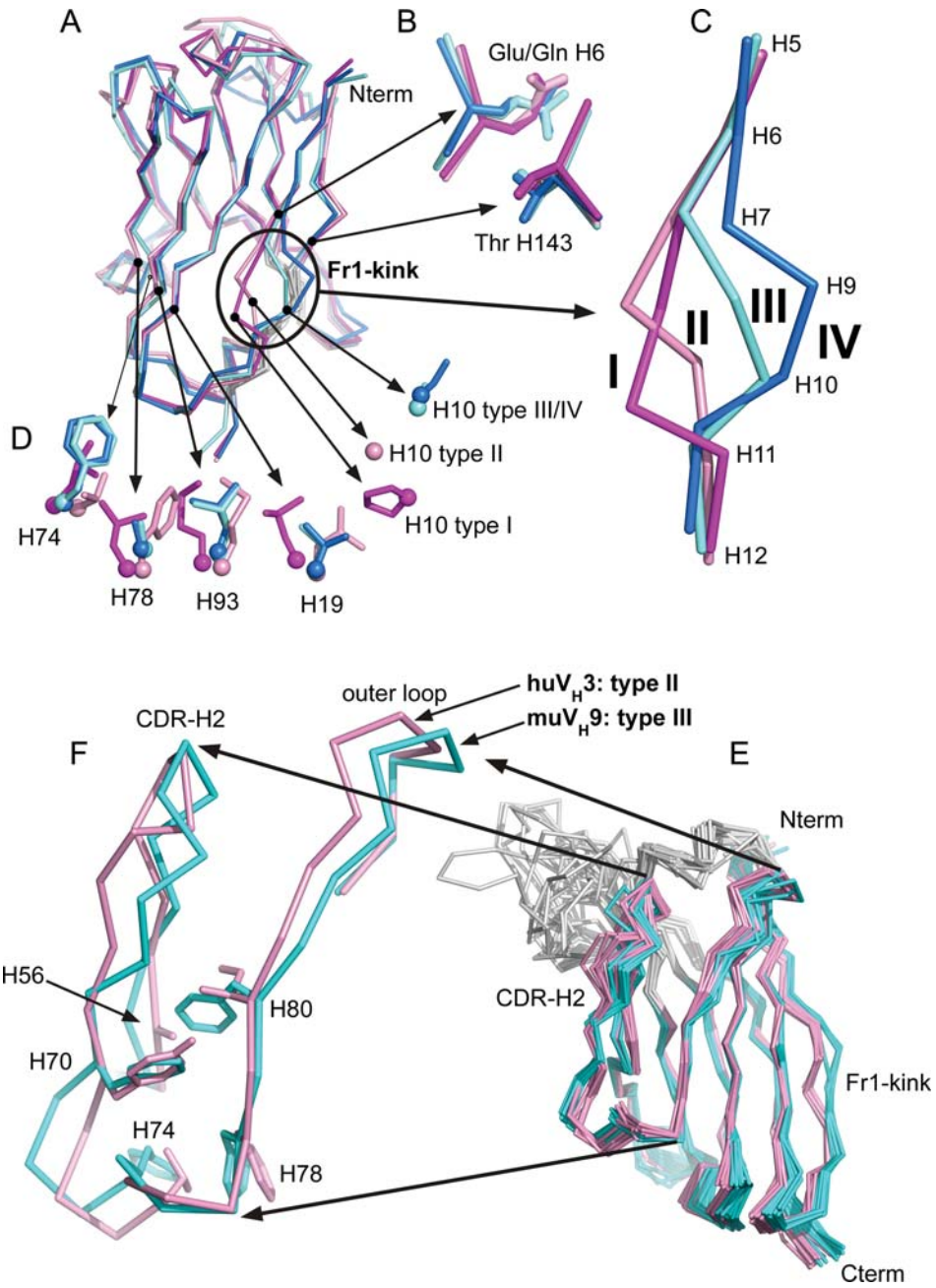

Fig. 1. Structural superposition of V_H domains. Coordinates of representative V_H domain structures for the four subtypes were excised from the structures of various antibody constructs downloaded from the PDB and aligned by least squares superposition of the structurally least variable C-positions in the V_H domain (H3–H6, H20–H24, H41–H47, H51–H57, H78–H82, H89–H93, H102–H108, H138–H144). The domains were color-coded according to the amino acids in positions H6, H7 and H10 predicting the structural subtype: magenta (type I): H6=E, H7 ≠ P, H10=P, represented by the V_H domain of PDB entry 1A7Q; pink (type II): H6=E, H7 ≠ P, H10=G, PDB entry 1AQK (Faber *et al*., 1998); cyan (type III): H6=Q, H7 ≠ P, PDB entry 12E8 (Trakhanov *et al*., 1999); blue (type IV): H6=Q, H7=P, first molecule in PDB entry 1CIC (Bentley *et al*., 1990). (**A**) Cα trace of entire V_H domain, (**B**) Glu/Gln H6 and Thr H143 side-chain conformation, (**C**) framework 1 main-chain conformation, (**D**) correlated structure and sequence changes across the V_H domain core. (**E**) Comparison of 12 representative structures derived from muV$_H$9 (magenta) and huV$_H$3 (cyan) germline domains after least squares superposition of just the inner β-sheet (residues H20–H24, H41–H47, H102–H108, H138–H144). It highlights the subtle differences in the relative orientations of the inner and outer β-sheet correlated with the domain subtype. (**F**) Differences in length, conformation and take-off angle of CDR-H2 between huV$_H$3 [pink, PDB entry 1AQK (Faber *et al*., 1998)] and muV$_H$9 [cyan, PDB entry 1N4X (Lescar *et al*., 2003)]. The figures were generated using the program PyMOL (http://pymol.sourceforge.net/).

of available huV$_H$3 and muV$_H$9 structures (Fig. 1E and F), we constructed a further chimeric acceptor framework from huV$_H$3 and muV$_H$9 elements: it retains the subtype-determining framework 1 residues and the hydrophobic core residues of the murine CDR donor Moc31 in combination with the surface residues specified by the huV$_H$3 consensus. This approach yielded the humanized scFv 4D5MocB (Willuda *et al*., 1999). This is summarized in Fig. 4.

Fears that the framework subtype might affect antigen binding, for example, by enforcing a different conformation on the CDRs, turned out to be unfounded in the case of the scFv Moc31: both variants, 4D5MocA and 4D5MocB, recognized

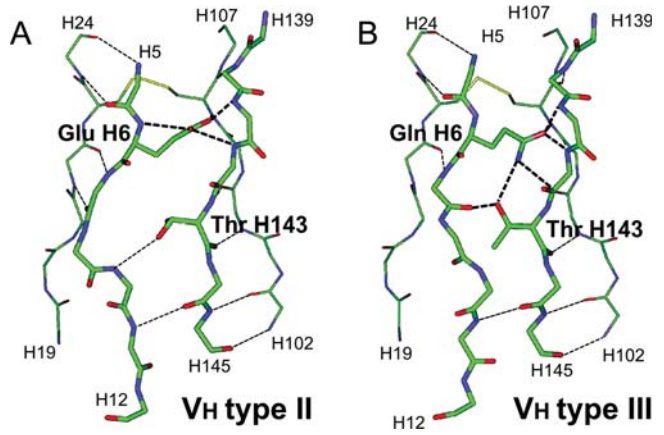

Fig. 2. Detailed view of the hydrogen bonding pattern involving the side chain of residue H6. (**A**) Type II consensus hydrogen bonding pattern (subtype signature H6=Glu, H7=not Pro, H10=Gly): one oxygen of the side-chain carboxylate group accepts two hydrogen bonds from the main-chain NH groups of Glu H6 and of Gly H142 (H106), the other from the main-chain NH groups of Cys H106 (H92) and of Gly H140 (H104). The side chain of Thr H143 (H107) is rotated relative to the conformation seen in the type III and IV structures. (**B**) Type III consensus hydrogen bonding pattern (subtype signature H6=Gln, H7=not Pro, H10=any amino acid): the oxygen of the side-chain amide can accept a hydrogen bond from two of the three main-chain NH groups of residues Gly H142 (H106) and Gly H140 (H104), which form the conserved β-bulge in FR-H4, and from Cys H106 (H92). The side-chain amide nitrogen of Gln H6 donates a hydrogen bond to the main chain carbonyl of Tyr H104 (H90) and to the side-chain hydroxyl group of Thr H143 (H107), which in turn donates a hydrogen bond to the main-chain carbonyl of Pro H7.

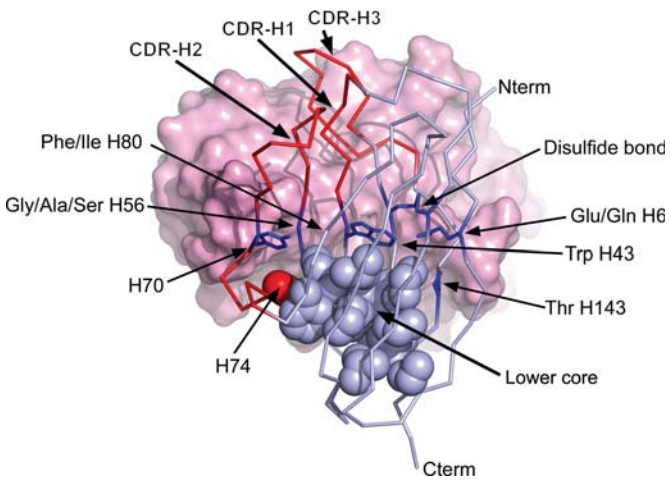

Fig. 3. Model structure. The V_H domain of the huVκ3-huV$_H$3·MocB model is shown as C-trace (pale blue), the V_L domain as solvent accessible surface (pink). The three CDRs of V_H are shown in red [CDR boundaries according to Kabat *et al.* (1991)]. The side chains of the hydrophobic lower core residues are shown in space filling (CPK) representation, the center core residues that separate the upper core from the lower core in stick representation (dark blue). The figure was generated using the program PyMOL (http://pymol.sourceforge.net/).

the antigen with comparable affinity. However, while both constructs showed significantly improved functional stability and production yield compared to the parental murine scFv, the functional stability of 4D5MocB, the loop graft to the chimeric framework, was considerably higher than that of the classical CDR graft 4D5MocA, as shown by a significantly increased half-life at 37°C (Willuda *et al.*, 1999). This additional stability

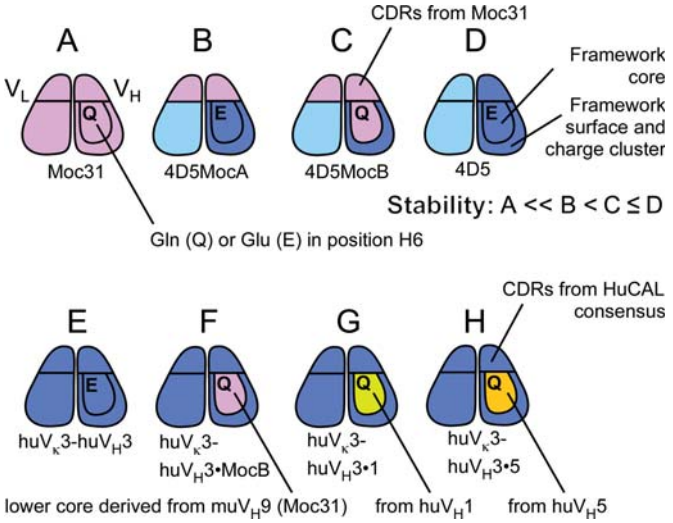

Fig. 4. Schematic representation of the scFv compared previously (Willuda *et al.*, 1999), (**A**) Moc31, (**B**) 4D5MocA, (**C**) 4D5MocB, (**D**) 4D5 and their relationship to the scFv analyzed in this study, (**E**) huVκ3-huV$_H$3, (**F**) huV$_H$3·MocB, (**G**) huVκ3-huV$_H$3·1 and (**H**) huVκ3-huV$_H$3·5. The regions considered in this study (CDRs, core, and framework surface) are indicated and colored according to their origin.

was crucial, as it resulted in a significantly improved biodistribution of the radiolabeled scFv in tumor targeting experiments on mouse xenografts, and allowed the further development of the 4D5MocB scFv into the ETA-immunotoxin (Di Paolo *et al.*, 2003) currently in phase III clinical trials for the treatment of head and neck cancer under the name of Proxinium™ and in phase II clinical trials for the treatment of bladder cancer under the name of Vicinium™ [Viventia Biotech Inc. (http://www.viventia.com)].

In this paper, we investigate the reasons for the improved functional stability of the chimeric V_H framework of 4D5MocB compared to the huV$_H$3 consensus framework used in 4D5MocA. This raises the more fundamental question whether there are better solutions to a stable, well-behaved framework than nature has found in huV$_H$3. We therefore specifically wanted to find out whether the superior biophysical properties of this huV$_H$3/muV$_H$9 chimeric V_H framework, compared to the consensus huV$_H$3 framework, were due to superior intrinsic properties of this chimeric framework or to destabilizing interactions between the Moc31 CDRs and the huV$_H$3 framework. To this end, we constructed three different chimeric V_H frameworks, each combining the core and subtype-determining residues of a different subtype III V_H domain with the surface residues and lower core charge cluster specified by the huV$_H$3 consensus (Fig. 4).

The first of these frameworks reproduces the huV$_H$3/muV$_H$9 chimera of the 4D5MocB framework (huV$_H$3·MocB), the second combines the core residues of the huV$_H$1 consensus with the huV$_H$3 framework (huV$_H$3·1) and the third investigates the combination of huV$_H$5 with huV$_H$3 (huV$_H$3·5). In order to be able to directly compare these constructs to the human consensus constructs (Ewert *et al.*, 2003), the CDR and upper core sequences were taken from the consensus huV$_H$3 HuCAL® fragment and the different chimeric V_H constructs were combined with the consensus huVκ3 domain to produce scFv fragments (Table I).

Table I. Summary of properties of scFv variants

Construct	Yield[a]	$[GdmCl]^b_{50}$	Thermal denaturation $t^c_{\frac{1}{2}}$	
	mg/l·OD_{10}	M	h (37°C)	h (65°C)
huV_k3-huV_H3	21	2.6	>92	~24
huV_k3-huV_H3·MocB	15.8	2.7	>92	~24
huV_k3-huV_H3·1	16.8	2.2	>92	<<24
huV_k3-huV_H3·5	11.6	2.4	>92	<<24
4D5	1–2[d]	1.4/2.8[e]	n.d.	n.d.
Moc31	0.2[d]	n.d.	<<0.5[d]	n.d.
4D5MocA	0.4[d]	n.d.	10[d]	n.d.
4D5MocB	1[d]	n.d.	>20[d]	n.d.

[a]Yield of soluble protein expressed in the periplasm of *E. coli*, normalized to OD_{600nm} of 10.
[b]Midpoint of the equilibrium denaturation trace (cf. Fig. 7).
[c]Half-life of disappearance of monomeric species at the temperature indicated.
[d]From Willuda *et al*. (1999).
[e]From Jäger *et al*. (2001), two transitions observed, second transition=V_L domain.

Materials and methods

Constructs

Starting from an scFv gene containing the synthetic HuCAL consensus domains huVκ3 and huV_H3 (Knappik *et al*., 2000), connected by a $(Gly_4Ser)_4$ linker in the vector pAK400 (Krebber *et al*., 1997), the three core-grafted V_H variants were produced by six successive mutagenesis steps using the *Dpn*I overlapping primer mutagenesis protocol (Quick-Change® site-directed mutagenesis kit, Stratagene). All constructs carried the same CDR-L3 and CDR-H3 derived from hu4D5-8 (Eigenbrot *et al*., 1993). In three mutagenesis steps, the mutations common to all three core grafts were introduced: Glu-H6-Gly and Gly-H10-Ala (step 1), Val-H55-Met and Ser-H56-Gly (step 2) and Val-H74-Phe (step 3). The resulting master mutant was sequenced, and the mutations differentiating the core-grafted variants were introduced by three more mutagenesis steps: the mutations Leu-H19-Val and Leu-H21-Ile (step 4a), Met-H93-Ile (step 5a) and Val-H145-Leu (step 6a) yielded the variant huV_H3·MocB, the mutations Leu-H19-Val and Leu-H21-Val (step 4b), Phe-H78-Val (step 5b) and Leu-H91-Met and Met-H93-Leu (step 6b) yielded the variant huV_H3·1, and the mutations Leu-H21-Ile (step 4c), Phe-H78-Val (step 5c) and Met-H93-Trp (step 6c) yielded the variant huV_H3·5.

The single domains, huVκ3 and the V_H, were expressed from the vector pJB33 (Ewert *et al*., 2003). scFv fragments consisting of the HuCAL huVκ3 consensus domain, a $(Gly_4Ser)_4$-linker and one of the V_H variants described above were assembled into the expression plasmid pAK400 (Krebber *et al*., 1997) in the V_L-linker-V_H format. All constructs contained a pelB signal sequence for export to the periplasm, followed by the sequence DSK and then the V_L-linker-V_H sequence and a C-terminal His_6 tag to allow IMAC purification.

Expression and purification

scFv fragments and isolated domains were expressed and purified in the same way. Thirty milliliters of dYT medium (16 g tryptone, 10 g yeast extract and 5 g NaCl per 1 l H_2O) containing 30 μg/ml chloramphenicol and 1.0% glucose were inoculated with a freshly transformed single colony of *E. coli* SB536 (Bass *et al*., 1996) and shaken overnight at 25°C. One liter of dYT medium (containing 30 μg/ml chloramphenicol and 50 mM K_2HPO_4) was inoculated with the pre-culture and incubated at 25°C in a 5 l flask with baffles and shaken at 105 rpm. Expression was induced at an OD_{550} of 1.0 by the addition of IPTG to a final concentration of 0.5 mM. Incubation at 25°C continued for 10 h; the cell density typically reached an OD_{550} between 4 and 6.5, with cells starting to lyse upon longer incubation times. Cells were collected by centrifugation (8000*g* for 15 min at 4°C), resuspended in 50 ml of 50 mM Tris–HCl (pH 7.5) containing 500 mM NaCl and disrupted by French press lysis. The crude extract was centrifuged (15 000*g* for 60 min at 4°C) and the supernatant passed through a 0.2 μm filter. The proteins were purified using an immobilized metal ion affinity chromatography (IMAC) column as described below. Pooled fractions were dialyzed against 10 mM MES (pH 6.0) and loaded onto an HS cation exchange column. Elution from the cation exchange column was achieved with a gradient from 0 to 3 M sodium chloride. Pooled fractions were dialyzed against 50 mM sodium phosphate (pH 7.0) containing 100 mM NaCl. The protein concentrations were determined by measuring the absorption at OD_{280} using the calculated extinction coefficient (Gill and von Hippel, 1989).

Assay for soluble expression and quantification of the scFv production yield

The above expression protocol was scaled down to 200 ml. All four scFv fragments ($huV\kappa3$-huV_H3, $huV\kappa3$-huV_H3·MocB, $huV\kappa3$-huV_H3·1 and $huV\kappa3$-huV_H3·5) were purified in parallel using bench-top IMAC batch purification (Qiagen Ni-NTA Superflow). A series of washes were performed, starting with a high salt wash (10 column volumes (c.v.) of 50 mM sodium phosphate, 1 M NaCl), followed by a low salt phosphate buffer wash (15 c.v. of 50 mM sodium phosphate, 100 mM NaCl). A series of low concentration imidazole washes (6 c.v. each of 20, 40 and 60 mM imidazole in low salt phosphate buffer) were applied to eliminate weakly binding contaminants before finally eluting with 250 mM imidazole. All washes and elutions were done at pH 7.5. The proteins were dialyzed against phosphate buffer (50 mM phosphate, 100 mM NaCl, pH 7) and quantified as above, using absorbance at 280 nm.

Gel filtration chromatography

Using the Ettan system (Amersham Biosciences), samples of purified scFv fragments were analyzed on a Superdex-75 column (Pharmacia) equilibrated with 50 mM sodium phosphate (pH 7.0) containing 500 mM NaCl. The proteins were injected at a concentration of 5 μM in a volume of 50 μL, with a flow rate of 60 μL/min. Cytochrome c (12.4 kDa), carbonic anhydrase (29 kDa), and bovine serum albumin (66 kDa) were used as molecular mass standards. For characterization of the half-life at elevated temperatures, a 5 μM stock of each protein was incubated at the temperature indicated, and aliquots were analyzed by gel filtration after various time intervals.

Equilibrium denaturation/renaturation experiments

Fluorescence spectra were recorded at 20°C with a PTI Alpha Scan spectrofluorimeter (Photon Technologies, Inc.).

Protein/GdmCl mixtures (500 µl) containing a final protein concentration of 0.5 µM and denaturant concentrations ranging from 0 to 5 M GdmCl were prepared from freshly purified protein and a 8 M GdmCl stock solution (in 50 mM sodium phosphate, pH 7.0 containing 100 mM NaCl). Each final concentration of GdmCl was determined by measuring the refractive index. The samples were incubated overnight at 20°C and the fluorescence emission spectra were then recorded from 320 to 370 nm with an excitation wavelength of 280 nm. Slit widths of 2 nm were used both for excitation and emission. The emission maximum was plotted as a function of GdmCl concentration. Apparent ΔG_{H2O}, m-values (slope of transition) and $[GdmCl]_{50}$ (the concentration of denaturant at which half of the protein is unfolded) values were obtained by applying a standard two-state fit of the wavelength of the emission maximum as a function of denaturant concentration (Creighton, 1997; Monsellier and Bedouelle, 2005) (eq. 1):

$$\lambda \max_{(obs)} = \frac{(\lambda \max_N + m_N \cdot [D]) + (\lambda \max_U + m_U \cdot [D]) \cdot e^{-(\Delta G_{H2O} - m \cdot [D])/RT}}{1 + e^{-(\Delta G_{H2O} - m \cdot [D])/RT}} \quad (eq.1)$$

Here $\lambda max_{(obs)}$ is the observed fluorescence maximum at a given denaturant concentration [D], λmax_N and m_N are intercept and slope of the pre-transition baseline, and λmax_U and m_U the same for the post-transition baseline, ΔG_{H2O} the free energy of unfolding at zero denaturant and m the dependence of free energy of unfolding on denaturant concentration. Since there is no strict proportionality between the shift of the spectral maximum and the fraction of folded and unfolded molecules, Monsellier and Bedouelle (2005) proposed a method to correct for the effects of the different quantum yields of the native and the denatured state. For the scFv fragments analyzed in this study, this correction factor turned out to be negligible (Supplementary data are available at *PEDS* online, Figure S2–S7 and Tables ST1–ST4).

Kinetic denaturation experiments

Protein/GdmCl mixtures (500 µl) contained a final protein concentration of 1 µM. Denaturant concentrations ranging from 3.1 to 6 M GdmCl were prepared from a GdmCl stock solution (8 M, in 50 mM sodium phosphate, pH 7.0 and 100 mM NaCl). The GdmCl concentration in each sample was empirically determined by using the refractive index. The GdmCl buffers and protein samples were pre-incubated (in separate tubes) for at least 45 min at 20°C. After manual mixing of the two solutions (mixing time ca. 5 s), the fluorescence emission at 330 nm as a function of excitation at 280 nm was recorded with a PTI Alpha Scan spectrofluorimeter (Photon Technologies, Inc.) until the protein unfolding reaction reached equilibrium. Slit widths were 2 nm for both excitation and emission.

Results

To reconcile the observations that, on the one hand, huV_H3 is one of the most frequently used frameworks and gives rise to antibodies of usually good biophysical properties, yet on the other hand, that the huV_H3-muV_H9 chimeric framework performed much better than huV_H3 with a particular set of CDRs (Willuda *et al.*, 1999), we set out to systematically investigate further hybrid frameworks. The observed superior stability might be due to a higher intrinsic stability of the chimeric V_H framework or to the removal of destabilizing interactions between the huV_H3 core residues and the Moc31-derived CDRs in the chimeric V_H framework. We therefore reconstructed this chimeric framework in combination with a different set of CDRs derived from the huV_H3 germline family consensus (CDR-H1 and CDR-H2) and from the antibody 4D5 hu4D5-8 (CDR-H3) (Eigenbrot *et al.*, 1993). In addition, we tested whether this stability gain can also be obtained using core residues derived from the human consensus domains that belong to the same structural subtype as muV_H9, namely huV_H1 and huV_H5.

We therefore compared the consensus huV_H3 to three different chimeric constructs, huV_H3·MocB, huV_H3·1, and huV_H3·5, in which the framework core residues of huV_H3 had been replaced by different residue combinations (Figs. 4 and 5). In all three constructs, the kink connecting strands A′ and A″, i.e. the subtype II determining residues Glu-H6 and Gly-H10 of huV_H3, were replaced by the subtype III determining residues Gln-H6 and Ala-H10, as present in huV_H1 and huV_H5. In muV_H9, H10 is a Pro. This Pro, however, does not influence the kink conformation. Therefore, it was replaced by Ala in huV_H3·MocB. Residue H7 was kept as Ser and H9 as Gly in all constructs. The two substitutions in positions H6 and H10 are sufficient to alter the conformation of the framework I kink from type II to type III, but out-of-context changes of the kink conformation usually lead to a destabilization of the domain due to unfavorable interactions with the domain core (Jung *et al.*, 2001).

Therefore, the lower core of the huV_H3 framework, composed of residues H19, H21, H55, H56, H74, H78, H91, H93, H96, H102, H104 and H145 [shown schematically in Fig. 4, as space filling (CPK) representation in Fig. 3 and indicated by open triangles in the sequence alignment in Fig. 5], was replaced by the residue combinations characteristic for each of the three different type III V_H domains: in huV_H3·MocB, the lower core residues were replaced by those of the muV_H9 domain, reproducing the hybrid framework of the humanized antibody 4D5MocB (Willuda *et al.*, 1999), but in the context of the heavy chain CDRs of the huV_H3 consensus domain. This construct differs only by a single amino acid (H21, Ile in muV_H9, Val in huV_H7) from a hypothetical core lower graft using the core of the human huV_H7 consensus and could therefore alternatively be called $huV_H3{\cdot}7_{(V21I)}$. Note that huV_H7 can be treated as a member of the huV_H1 family, as was done in HuCAL (Knappik *et al.*, 2000). In huV_H3·1, the lower core residues were derived from the consensus of the human V_H1 germline family, in huV_H3·5 by those of the huV_H5 consensus framework.

As some of the 12 hydrophobic lower core residues are conserved between huV_H3 and the type III V_H domain serving as core donor, there are less than 14 sequence differences between huV_H3 and the three constructs: huV_H3 and huV_H3·MocB differ by 9 residues, huV_H3 and huV_H3·1 by 10 residues and huV_H3 and huV_H3·5 by 8 residues. Five of these substitutions are identical in all three hybrid constructs: the subtype-determining residues H6 and H10, changing

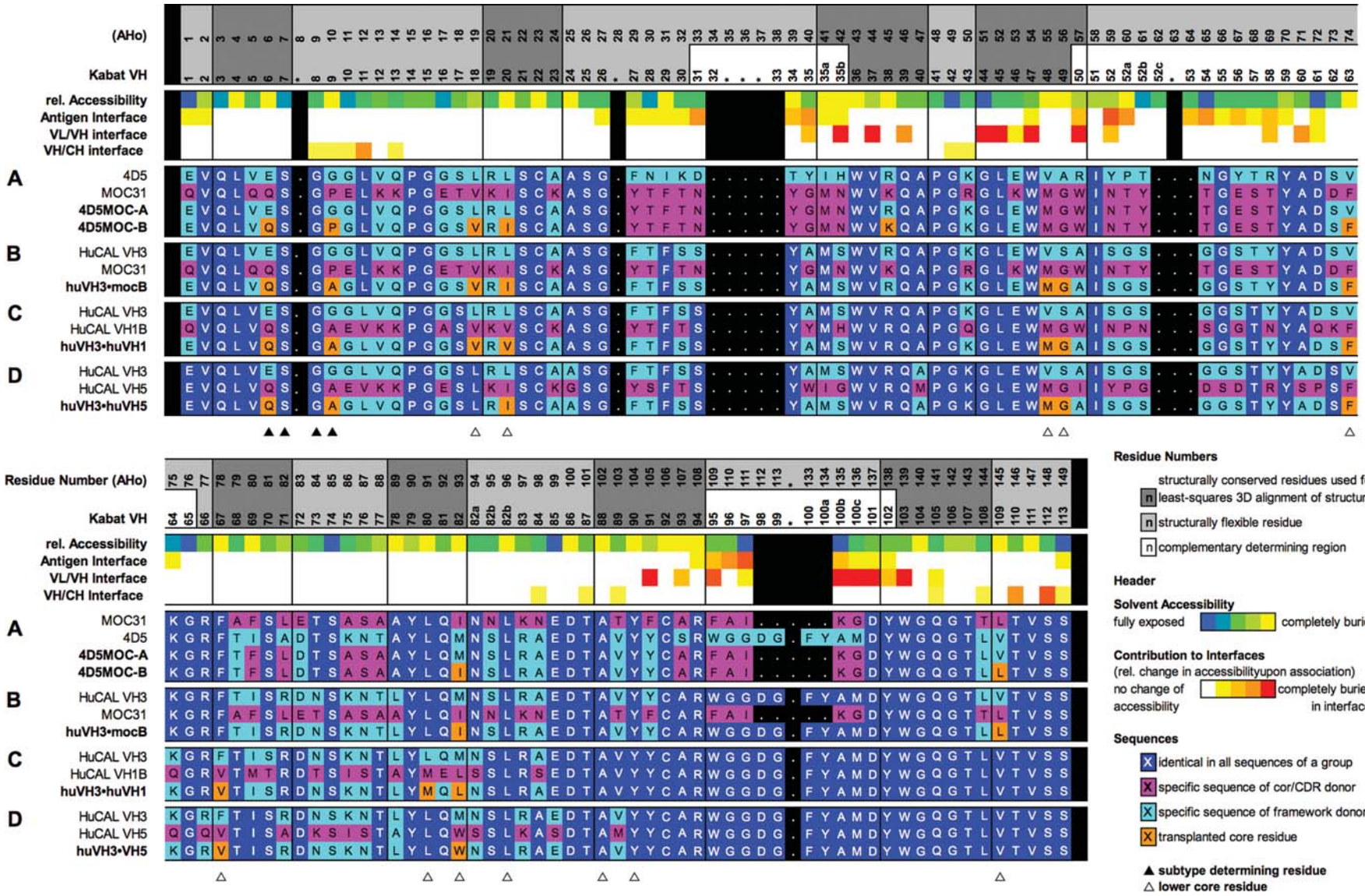

Fig. 5. Sequence alignment. (**A**) Sequences of the V_H domains involved in the Moc31/huV$_H$3 CDR-grafts: acceptor framework *4D5*, CDR donor *Moc31*, classical CDR-graft *4D5MocA* and CDR-graft *4D5MocB* retaining the Moc31 hydrophobic core residues. (**B**) Lower core graft from the V_H domain of Moc31 to HuCAL huV$_H$3: acceptor framework *HuCAL huV$_H$3*, core donor *Moc31*, core graft *huV$_H$3·MocB*. (**C**) Lower core graft from the V_H domain of HuCAL huV$_H$1 to HuCAL huV$_H$3: acceptor framework HuCAL *huV$_H$3*, core donor HuCAL *huV$_H$1*, core graft *huV$_H$3·1*. (**D**) Lower core graft from the V_H domain of HuCAL huV$_H$5 to HuCAL huV$_H$3: acceptor framework HuCAL *huV$_H$3*, core donor HuCAL *huV$_H$5*, core graft *huV$_H$3·5*. In each group of sequences, those residues that are identical in all sequences are shown in white on a dark blue background, residues carrying the specific sequence of the acceptor framework are shown in black on a cyan background and residues carrying the specific sequence of the CDR- or core donor are shown in black on magenta. The grafted core residues are highlighted by an orange background. In the header of the alignment, the residue numbers according to the AHo (Honegger and Plückthun, 2001a) and the Kabat (Kabat *et al*., 1991) numbering scheme are indicated. Color codes show the average solvent exposure of the residues in an isolated V_H domain relative to the same amino acid in the context of an extended poly-Ala chain (yellow, >10%; yellow–green; 10–25%, green, 25–50%; dark green, 50–75%; green–blue 75–100%; blue, >100%) and the average relative reduction in solvent accessible surface upon complex formation between antibody and antigen, between V_L and V_H domain and between variable and constant domains (red, >80%; red–orange, 60–18%; orange, 40–60%; yellow–orange, 20–40%; yellow, >0–20%; white, 0%).

the kink sequence signature of residues H6–H10 from Glu-Ser-Gly-Gly to Gln-Ser-Gly-Ala, the substitutions Val-H55 to Met and Ser-H56 to Gly, affecting the β-bulge at the start of CDR-H2 and Val-H74 to Phe, a residue formally located within CDR-H2, but structurally part of the lower core (Figs 3 and 5). All CDR and upper core residues, surface residues, semi-exposed Val-H13 and the charge cluster comprising the buried salt bridge between Arg-H77 and Asp-H100, Arg H45 and Glu H53, Asp H72 and Lys H75, Arg H97 and Glu H99 were retained from huV_H3 as embodied in the HuCAL V_H3 consensus domain.

Expression yields of scFv fragments

Ideally, one would directly compare the properties of the isolated V_H domains. However, these isolated domains are highly aggregation-prone due to the hydrophobic surface, which forms the V_H/V_L interface in a scFv but is solvent exposed in the isolated domain. Since $huV_H3{\cdot}1$ and $huV_H3{\cdot}5$ could not be produced as isolated domains, and preparations of $huV_H3{\cdot}$MocB always contained a sizable fraction of aggregates, huV_H3 and the three core grafts were each combined with the most stable of the human V_L consensus domains, huVκ3, to form an scFv in V_L-$(Gly_4Ser)_4$-V_H orientation with a C-terminal His-tag, and inserted into the vector pAK400 (Krebber *et al*., 1997) for periplasmic expression in *E. coli*. The consensus scFv fragment huVκ3-huV_H3 and the core grafts huVκ3-$huV_H3{\cdot}$MocB, huVκ3-$huV_H3{\cdot}1$, and huVκ3-$huV_H3{\cdot}5$ and a reconstructed huVκ3-huV_H3 in the same orientation and vector were purified under non-denaturing conditions after expression in soluble form in the periplasm.

With a soluble expression yield of 10–20 mg of pure protein from a 1 l culture normalized to an $OD_{600\ nm}$ of 10 (in short, mg/l·OD_{10}), the yields of these four constructs were significantly higher than the yields obtained for the original Moc31 scFv [0.2 mg/l·OD_{10}, which can be increased to 0.6 mg/l·OD_{10} by coexpression of the chaperone Skp (Bothmann and Plückthun, 1998)]. This can be compared with the control scFv hu4D5 (1–2 mg/l·OD_{10}), and the humanized Moc31 scFv fragments 4D5MocA (0.4 mg/l·OD_{10}) and 4D5MocB (1 mg/l·OD_{10}) (Willuda *et al*., 1999). The expression yields of the three core-grafted constructs huVκ3-$huV_H3{\cdot}1$ (16.8 mg/l·OD_{10}), huVκ3-$huV_H3{\cdot}$MocB (15.8 mg/l·OD_{10}), and huVκ3-$huV_H3{\cdot}5$ (11.6 mg) were slightly lower than that of the full consensus huVκ3-huV_H3 (20.9 mg/l·OD_{10}). This yield was well above the 6.5 mg/l·OD_{10} reported (and confirmed here) for the huV_H3-huVκ3 construct in the pMorphX7 vector (Ewert *et al*., 2003).

Side-by-side comparison of the two consensus constructs confirmed that the V_L-linker-V_H scFv in pAK400 (Krebber *et al*., 1997) reproducibly gave higher yields when normalized to OD than V_H-linker-V_L scFv composed of the same V_L and V_H domains in pMorphX7 (Morphosys AG) (Knappik *et al*., 2000) (21 mg/l·OD_{10} for huVκ3-huV_H3 in pAK400 vs. 5.8 mg/l·OD_{10} for huV_H3-huVκ3 in pMorphX7). However, cells containing the same scFv construct in the vector pMorphX7 grew to up to two times higher density in standard shaking flask culture without starting to lyse than cells containing the pAK400 vector, making the net yield per liter of culture more similar between the vectors.

In V_H-linker-V_L orientation and the pMorphX7 vector, the consensus constructs of the core donors huV_H1a-huVκ3 (11.1 mg/l·OD_{10}) and huV_H1b-huVκ3 (12.4 mg/l·OD_{10}) yielded twice as much protein as huV_H3-huVκ3 (6.5 mg/l·OD_{10}) in the same vector, while huV_H5-huVκ3 (6.5 mg/l·OD_{10}) was produced with approximately the same yield as huV_H3-huVκ3 (Ewert *et al*., 2003).

Functional stability of the scFv fragments

An scFv intended for use in biological assays and ultimately in therapeutic application has to be stable and remain functional at physiological temperatures and at high concentrations. The time course of aggregation upon incubation in buffer at 37°C or of loss of antigen binding activity upon incubation in serum at that temperature is frequently used as a measure to assess the ability of an scFv to withstand thermal stress under physiological conditions. Since the constructs analyzed in this study do not recognize a specific antigen, we could only assess the loss of soluble protein due to aggregation.

Gel filtration analysis of the freshly purified scFv fragments showed all four constructs to elute at the expected size (27 kDa) as monomers, with only a small shoulder hinting at the presence of a very minor fraction of dimers for huVκ3-$huV_H3{\cdot}$MocB and huVκ3-$huV_H3{\cdot}5$ (Fig. 6A). Thus, the different domain cores introduced into the V_H framework fragment did not result in a significant increase of dimer formation. Incubation at temperatures above the respective aggregation temperature resulted in the irreversible precipitation of the protein. The consensus scFv fragment huVκ3-huV_H3 and the core grafts huVκ3-$huV_H3{\cdot}$MocB, huVκ3-$huV_H3{\cdot}1$ and huVκ3-$huV_H3{\cdot}5$ all remained fully soluble and monomeric for more than 92 h at 37°C and for more than 48 h at 50°C. Interestingly, the dimer shoulder observed in freshly prepared material disappeared with concomitant increase of the monomer peak height upon incubation for 24 h at 50°C, presumably indicating the re-equilibration of dimer to monomer (Fig. 6B). This is consistent with previous observations of monomer being the thermodynamically preferred form at low to moderate concentrations (Arndt *et al*., 1998). After 24 h at 65°C, 44% of the huVκ3-huV_H3 and 34% of huVκ3-$huV_H3{\cdot}$MocB were recovered in the monomeric fraction, while less than 5% of huVκ3-$huV_H3{\cdot}1$ and huVκ3-$huV_H3{\cdot}5$ were recovered in the monomeric fraction. Thus, the thermal stability appears to be highest for huVκ3-huV_H3, closely followed by huVκ3-$huV_H3{\cdot}$MocB, while huVκ3-$huV_H3{\cdot}1$ and huVκ3-$huV_H3{\cdot}5$ were significantly less resistant to thermal aggregation. In contrast, at least 95% of the murine Moc31 scFv had aggregated within 30 min at 37°C, the loop-graft 4D5MocA showed a half-life of around 10 h at 37°C and only the core-engineered 4D5MocB showed no measurable aggregation or precipitation after 20 h at 37°C (Willuda *et al*., 1999).

Equilibrium unfolding of the scFv fragments in guanidinium chloride

Since scFv fragments aggregate and precipitate upon thermal denaturation, the relative equilibrium thermodynamic stabilities of the different constructs were instead assessed by chemical denaturation, observing the change of the tryptophan fluorescence emission spectrum as a function of guanidinium concentration (Eftink, 1994). The equilibrium denaturation was entirely reversible, as unfolding and

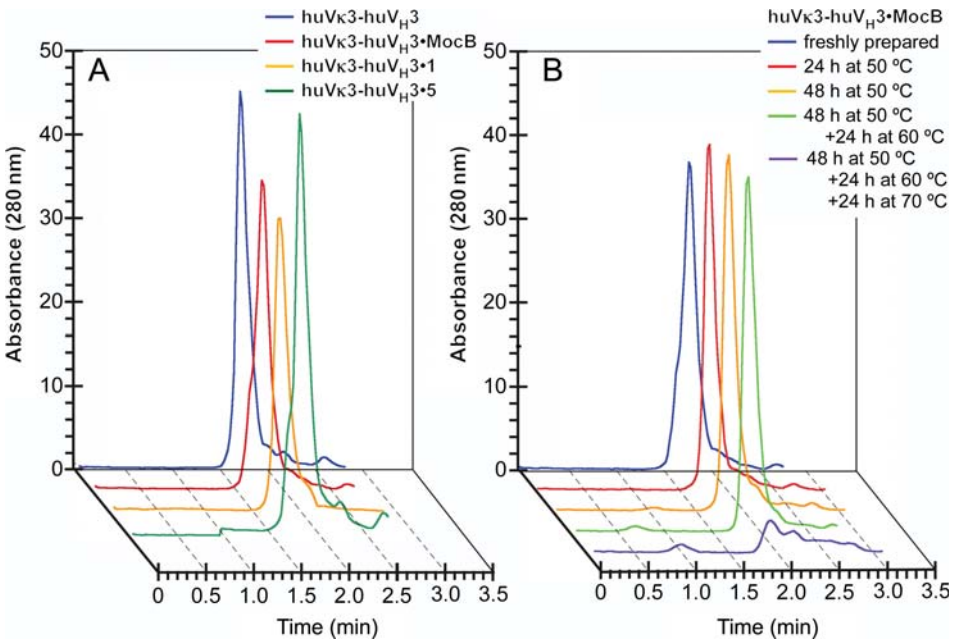

Fig. 6. Gel filtration profiles (**A**) of freshly purified huVκ3-huV$_H$3, huVκ3-huV$_H$3·MocB, huVκ3-huV$_H$3·1 and huVκ3-huV$_H$3·5; (**B**) of aliquots of huVκ3-huV$_H$3·MocB freshly purified, after 24 h at 50°C, after 48 h at 50°C, after 48 h at 50°C and 24 h at 60°C, and after 48 h at 50°C, 24 h at 60°C and 24 h at 70°C.

refolding curves, starting from the completely folded or unfolded protein, respectively, were superimposable (Supplementary data are available at *PEDS* online, Figure S4). The net change in fluorescence quantum yield upon denaturation was small. The fluorescence intensity data showed large errors between closely spaced data points, presumably due to light scattering by aggregated species at intermediate denaturant concentrations.

We therefore resorted to an analysis of the spectral shift of the emission maximum (wavelength of the emission maximum or center of spectral mass). This has been shown to give more robust values for scFv proteins, as this parameter is not affected by light scattering (Wörn and Plückthun, 1999) of soluble aggregates that may form at intermediate denaturant concentrations. The $[GdmCl]_{50}$ values should therefore be interpreted as the midpoint of the observable spectral shift upon unfolding. If the scFv fragment does not follow a two-state transition, this should not be interpreted as the denaturant concentration at which 50% of the scFv is fully unfolded. Deviations from two-state behavior are frequent for scFv fragments [Supplementary data are available at *PEDS* online, Figure S6 and (Wörn and Plückthun, 1999; Röthlisberger *et al*., 2005)].

Comparison of the denaturation curves of the different constructs (Fig. 7) shows that the denaturation curves of the two reference scFv with opposite domain orientation, huV$_\kappa$3-huV$_H$3 and huV$_H$3-huVκ3, do not differ significantly from each other and agree with the value determined previously (Ewert *et al*., 2003) for huV$_H$3-huVκ3. The reference curves for huV$_H$1-huVκ3 and huV$_H$5-huVκ3 were, therefore, also taken from previously described experiments (Ewert *et al*., 2003). Vκ3-huV$_H$3 ($[GdmCl]_{50}$=2.6 M) and huVκ3-huV$_H$3·MocB ($[GdmCl]_{50}$=2.7 M) show very similar denaturation midpoints (Fig. 7A), although, reflected in a steeper transition of the equilibrium folding/unfolding curve of huVκ3-huV$_H$3·MocB (higher apparent cooperativity), this construct starts to unfold at a somewhat higher denaturant concentration than the reference construct. In contrast, huVκ3-huV$_H$3·5 unfolds with a $[GdmCl]_{50}$ of 2.4 M, intermediate between that of huVκ3-huV$_H$3 (2.6 M) and that of the core donor huV$_H$5-huV$_k$3 (2.2 M) (Fig. 7C), and huVκ3-huV$_H$3·5 (2.2 M) unfolds at lower denaturant concentration than either huVκ3-huV$_H$3 or huVκ3-huV$_H$3·1 (2.4 M) (Fig. 7B).

Upon denaturation, the wavelength of the fluorescence maximum of the scFv is shifted by ~12 nm. The use of this measure of unfolding in the determination of ΔG of unfolding needs special caution. Differences in the shape of the spectrum and in the fluorescence quantum yield of the native and the denatured state can lead to deviation from a strict proportionality between the spectral shift and the fraction of molecules that have undergone the transition from the native to unfolded state (Monsellier and Bedouelle, 2005). Although Monsellier and Bedouelle suggest a corrective term involving the curvature of the spectra at their λmax that would allow to correct for the non-linear dependence of fluorescence emission maximum on the fraction of molecules that are unfolded (Monsellier and Bedouelle, 2005), we hesitate to extrapolate to $\Delta G_{(H2O)}$ from these curves, as we have reason to believe that a two-state model of unfolding does not adequately describe the unfolding transitions of all of our scFv.

The data showed a good fit to a two-state model (Creighton, 1997) (cf. Eq. 1), with *r*-values of 0.999 or better. However, while the *m*-value of 7.4 kcal·l/mol^2 for huVκ3-huV$_H$3·MocB approaches the value that would be expected according to Myers *et al.* (1995) for a protein of 28 kDa with two disulfide bonds such as an scFv, an *m*-value of 2.7 kcal·l/mol^2, as observed for huVκ3-huV$_H$3, would be expected for a protein of only ~14 kDa with two disulfide bonds. The four scFv investigated in this study differ from each other only by a small number of rather conservative point mutation.

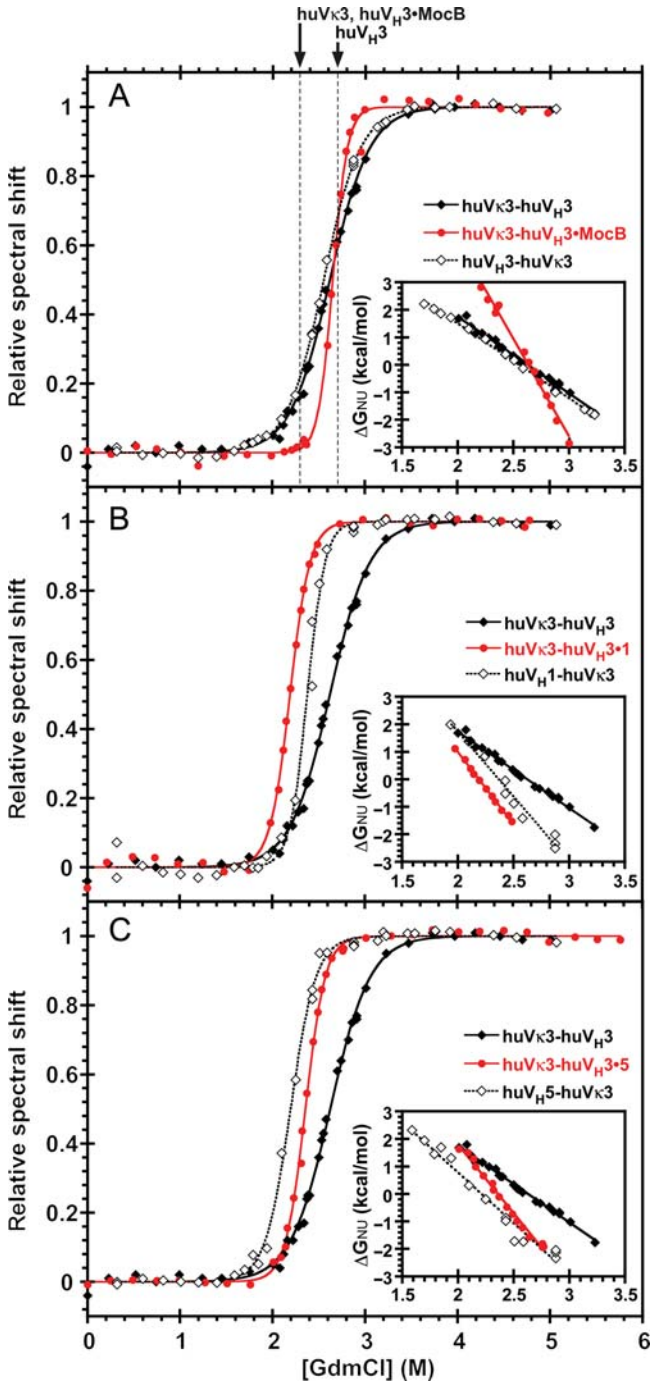

Fig. 7. GdmCl denaturation curves of the scFv constructs, compared to the closest HuCAL® human consensus scFv fragments. (**A**) Consensus scFv huVκ3-huV$_H$3 (this study) and huV$_H$3-huVκ3 (Ewert *et al.*, 2003) compared to the scFv containing the muV$_H$9 lower core graft huVκ3-huV$_H$3·MocB. Dashed vertical lines indicate the denaturation midpoints of the isolated huVκ3 and huV$_H$3 domains and the approximate denaturation midpoint of huV$_H$3·MocB. (**B**) Consensus scFv huV$_H$1-huVκ3 (Ewert *et al.*, 2003) compared to huV$_H$1 lower core graft huVκ3-huV$_H$3·1 and scFv huVκ3-huV$_H$3. (**C**) Consensus scFv huV$_H$5-huVκ3 (Ewert *et al.*, 2003) compared to huV$_H$5 lower core graft huVκ3-huV$_H$3·5 and scFv huVκ3-huV$_H$3. The unfolding transitions were observed by following the change of the wavelength of the emission maximum of the Trp fluorescence (excitation wavelength 280 nm) as a function of denaturant concentration. The data were fitted using the two-state model (Santoro and Bolen, 1988), simultaneously fitting the pre-transition-baseline (λmax_N, m_N), the post-transition baseline (λmax_U, m_U) and the thermodynamic parameters $\Delta G_{(H2O)}$ and *m* and plotted as relative spectral shift (relative change of $\lambda max_{(obs)}$ vs. denaturant concentration after baseline correction). Insets show plots of the fitted $\Delta G_{(GdmCl)}$ vs. denaturant concentration for those points whose relative spectral shift lay between 0.05 and 0.95. However, since we find evidence that the two-state assumption is not fulfilled in this system (see text), we do not report the fitted ΔG values. Plots of the raw λmax vs. [GdmCl] data for the equilibrium unfolding and refolding reaction, the apparent thermodynamic parameters derived from the fit, the spectra of the folded and unfolded scFv and the influence of corrections (Monsellier and Bedouelle, 2005, 2006) aimed at compensating for the spectral differences between the two states are provided in the Supplementary Material available at *PEDS* online.

The *m*-value can differ from the one expected for the molecular size if there is a hidden intermediate (i.e. it is not a two-state system). However, we first consider the possibility to explain the data within a two-state state approximation.

The *m*-value (cooperativity of unfolding) in a two-state system is related to the change in solvent accessible surface area (ΔASA) upon denaturation (Myers *et al.*, 1995). To explain large differences in *m*-value between closely related mutants, one has to postulate either differences in the strength of the interaction between the residues exposed upon unfolding and the denaturant (Tanford, 1970), which is unlikely for very closely related proteins, or that some mutants are not fully unfolded by the denaturant, which would result in different ΔASA. Our data would require a change in ΔASA by a factor 2 to 3 between the mutants.

However, we find that an incomplete denaturation of some mutants would not be consistent with our measurements: the slope of the post-transition baseline is very small and very similar for the different mutants, the emission maxima and the shape of the spectra of the unfolded scFvs are very similar for the four constructs (Supplementary data are available at *PEDS* online, Figures S2 and S3) and to what is expected for exposed Trp, arguing against a significant difference in the amount of residual structure in the unfolded state.

A very different *m*-value, taken literally, would mean to extrapolate from the denaturation midpoint to zero denaturant with a very different slope. The values so obtained are, however, clearly not consistent with the functional stabilities that we could measure directly in native buffer. Using a two-state fit with these different *m*-values, we would extrapolate for huVκ3-huV$_H$3 an apparent thermodynamic stability $\Delta G_{(H2O)}$ of only about 7 kcal/mol compared to around 17 kcal/mol for huVκ3-huV$_H$3·MocB, 11 kcal/mol for huVκ3-huV$_H$3·1 and 13 kcal/mol for huVκ3-huV$_H$3·5 (Supplementary data are available at *PEDS* online, Tables ST–ST3), while thermal aggregation experiments (see above) and kinetic denaturation experiments (see next section) suggest huVκ3-huV$_H$3 to be at least as stable as huVκ3-huV$_H$3·MocB. We thus do not believe that the scFv mutants are adequately described by a two-state approximation, and consequently do not believe that $\Delta G_{(H2O)}$ so obtained would be valid.

Based on previous studies (Wörn and Plückthun, 1999; Wörn *et al.*, 2000; Jäger *et al.*, 2001; Röthlisberger *et al.*, 2005), we suggest that true two-state unfolding behavior of an scFv is the exception rather than the rule, and is predominantly seen in scFv composed of domains that have low intrinsic stability but are stabilized to a significant extent in the scFv (Supplementary data are available at *PEDS* online, Figure S5a). Taken together, the low apparent *m*-values are most consistent with a hidden intermediate, which would

preclude to use such different *m*-values to extrapolate to zero denaturant to calculate $\Delta G_{(H2O)}$ in a comparison of mutants. The relative stability at medium denaturant concentration, indicated by the $[GdmCl]_{50}$ values, may thus at least qualitatively describe the relative stability of the mutants at zero denaturant. This only assumes that a similar extrapolation slope is used for all mutants.

Unfolding kinetics

The four scFv were mixed with different concentrations of GdmCl and the unfolding reaction was followed by recording the change in fluorescence intensity at 330 nm. Figure 8A compares the unfolding traces of the scFv fragments at a guanidinium concentration of 3.2 M, a concentration at which at equilibrium even the most stable construct was >95% denatured. The shape of the trace was different for the four constructs: huVκ3-huV$_H$3 showed a monotonous, slow drop in fluorescence intensity, huVκ3-huV$_H$3·MocB an initial fast drop followed by a slow increase and for huVκ3-huV$_H$3·1 and huVκ3-huV$_H$3·5, this initial drop was so fast that this first phase was essentially completed within the dead-time of manual mixing (5 s). The rate of the slow phase of fluorescence increase was not only the same for the three chimeric constructs, but was also identical to the unfolding rate of the isolated huVκ3 domain (Fig. 8B). huVκ3-huV$_H$3, huVκ3-huV$_H$3·MocB and huVκ3-huV$_H$3·1 showed similar specific fluorescence intensities in the native state and also tended towards the same fluorescence intensity in the denatured state. The specific fluorescence of huVκ3-huV$_H$3·5 was higher than that of the other three constructs due to an additional tryptophan residue in the huV$_H$5-derived core (Trp-H93).

Comparison of the spectra of native and denatured isolated huVκ3 and huV$_H$3 domain and of the scFv composed of these domains suggests that the conserved core Trp L43 and Trp H43 are highly quenched in the native domain. Thus, the fluorescence intensity increases as isolated huVκ3 and huV$_H$3 domains unfold (Jäger *et al*., 2001). The specific fluorescence of the scFv is higher than the sum of the fluorescence of the two isolated domains. Therefore, the contribution of the three V_H tryptophan residues buried in the interface between the between the V_L and the V_H domain, Trp H54 (conserved), H109 (CDR-H3) and H139 (conserved) is lower when these residues are solvent exposed (isolated domains) than when they are buried in the domain interface (scFv) (Location of the tryptophans in the scFv structure is shown in Supplementary data are available at *PEDS* online, Figures S1). Upon domain dissociation, not only does the fluorescence quantum yield of the interface Trp residues decrease, but also the fluorescence maximum shifts from lower wavelength to ~350 nm, the typical value for exposed tryptophan residues (Schmid, 2005). Both effects together explain the shift of the maximum of the huVκ3-V$_H$3 scFv from 338.4 nm for the native molecule to 349.2 nm for the fully denatured scFv in 5 M GdmCl, and the decrease of fluorescence intensity at 330 nm upon full or partially denaturation. The fast initial decrease of fluorescence intensity in the unfolding traces of huVκ3-huV$_H$3·MocB, huVκ3-huV$_H$3·1 and huVκ3-huV$_H$3·5 is, therefore, governed by the exposure of the interface tryptophans as a consequence of the unfolding of the V_H domains, while the subsequent increase in fluorescence intensity represents the unquenching of Trp L43 as the V_L domain unfolds. In V_H, the analogous unquenching of Trp H43 is masked by the fluorescence increase of Trp H54, Trp H109 and Trp H139 upon denaturation in the context of the scFv fragment.

In summary, the thermal stability and midpoint of chemical denaturation were very similar for the huVκ3-V$_H$3 and

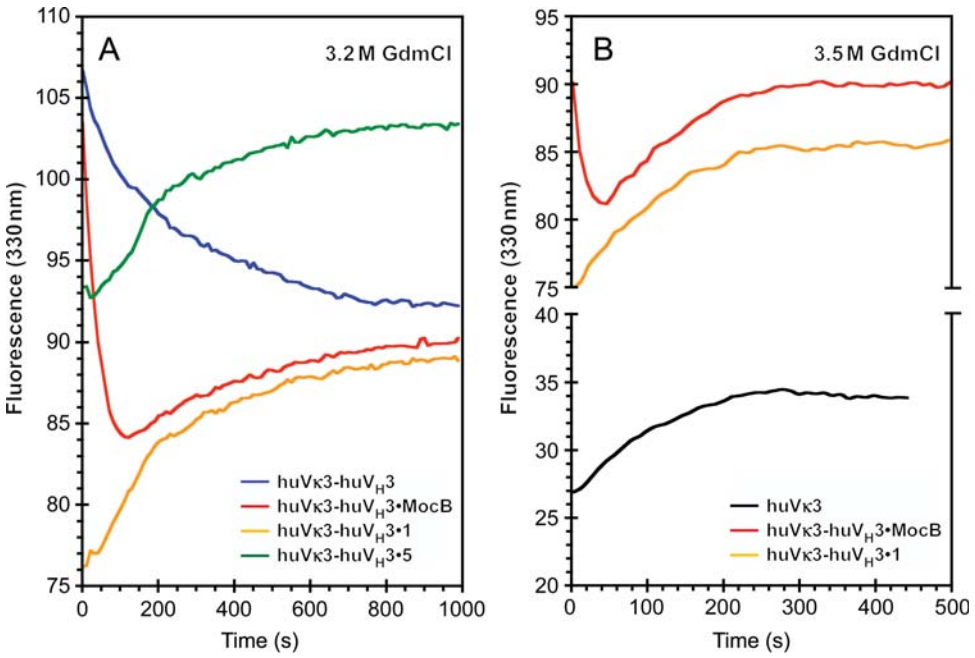

Fig. 8. Unfolding kinetics. (**A**) Unfolding kinetics of the scFv huVκ3-huV$_H$3, huVκ3-huV$_H$3·MocB, huVκ3-huV$_H$3·1 and huVκ3-huV$_H$3·5 in 3.2 M GdmCl. (**B**) Unfolding kinetics of the scFv huVκ3-huV$_H$3·MocB and huVκ3-huV$_H$3·1 and of the isolated huVκ3 domain in 3.5 M GdmCl. After manual mixing with a dead time of ~5 s, the unfolding was observed as a function of time by recording the change in fluorescence intensity at 330 nm with an excitation wavelength of 280 nm.

huVκ3-V$_H$3·MocB scFv. ScFv huVκ3-huV$_H$3·5 was less stable, and huVκ3-huV$_H$3·1 the least stable of the four constructs, consistent between the midpoint of denaturation and the thermal stability. The unfolding of the huV$_H$3·MocB domain was significantly faster than that of the huVκ3, indicating a higher activation energy of unfolding for the huVκ3 domain.

Discussion

When designing a CDR graft in order to humanize and/or to stabilize an antibody, one frequently has the choice to either graft to the human consensus framework most closely related to that of the CDR donor, or to the most stable of the human frameworks, the huV$_H$3 framework. While the subtype II containing huV$_H$3 is the largest human germline family, the murine antibody repertoire is dominated by frameworks of structural subtypes III and IV, due to the large number of muV$_H$1 germlines. Thus, in order to design the optimal CDR graft for a given murine sequence, the consequences of grafting to a structurally divergent framework have to be taken into account.

In previous studies (Willuda *et al*., 1999), two CDR-grafts from the muV$_H$9 (type III) V$_H$ domain of antibody Moc31 were compared. They were either to the consensus huV$_H$3 domain (type II) framework or to a chimeric framework that was derived from huV$_H$3, but whose structural subtype had been adapted to that of the CDR donor by retaining the subtype determining residues H6 and H10 and the hydrophobic core residues of the CDR donor (Fig. 4A–D). Although both grafts were significantly more stable than the parental murine scFv, the graft to a V$_H$ framework that retained the structural subtype of the CDR donor (4D5MocB), and therefore more closely resembled the parental antibody, was more stable than the graft to the consensus huV$_H$3 framework (4D5MocA).

Two different hypotheses can be formulated that might account for the observed differences in stability: (i) either the intrinsic stability of the chimeric framework of 4D5MocB is higher than that of the huV$_H$3 consensus framework of 4D5MocA, or (ii) destabilizing interactions between the muV$_H$9-derived CDRs and the consensus huV$_H$3 domain core might have reduced the stability of 4D5MocA. Hypothesis (i) would predict that the stability of grafts to the chimeric framework should be higher than that of grafts to the consensus huV$_H$3 domain, independent of the origin of the CDRs, while hypothesis (ii) would predict that the chimeric framework would only be superior if combined with CDRs derived from muV$_H$9, and possibly other type III V$_H$ domains. In contrast, in combination with huV$_H$3-derived CDRs and CDRs derived from other type II V$_H$ domains, the consensus huV$_H$3 domain would give rise to superior molecules. Either result would have implications beyond the system tested—if hypothesis (i) were correct, we would have a generally applicable way to improve the stability of problematic CDR grafts, while if hypothesis (ii) were correct, it would mean that the structural subtype of CDR donor and acceptor framework have to be matched when designing a CDR graft in order to produce a graft with the best possible biophysical properties.

To test the two hypotheses, we put both the consensus huV$_H$3 framework and the huV$_H$3-muV$_H$9 chimeric framework into a different context by combining them with huV$_H$3-consensus-derived CDR-H1 and -H2, a CDR-H3 taken from hu4D5-8, and providing the scFv with a huVκ3 consensus domain. In this context, hypothesis (i) would predict the scFv containing the chimeric V$_H$ framework to be more stable, while hypothesis (ii) would predict the scFv containing the consensus huV$_H$3 framework to be more stable. To test whether it was sufficient to convert the subtype of the V$_H$-framework from type II to type III, or whether the specific combination of hydrophobic core residues found in muV$_H$9 was needed, we added two more chimeric V$_H$ domains to the analysis. In one of these, the core residues were taken from the huV$_H$1 consensus, in the second, from the huV$_H$5 consensus. An added incentive for testing the latter two constructs lay in the observation that scFv huV$_H$1-huVκ3 gave higher and huV$_H$5-huVκ3 similar yields as the more stable huV$_H$3-huVκ3 upon periplasmic expression in *E. coli* (Ewert *et al*., 2004).

Thus, we compared the biophysical properties of four different scFv fragments which differed only in the subtype-determining residues and the hydrophobic residues of the lower core (Fig. 4E–H). In scFv huVκ3-huV$_H$3, all residues are derived from the consensus sequence of the corresponding human germline family, with the exception of CDR-L3 and CDR-H3, which were taken from hu4D5-8. In the other three scFv, glutamate H6 was replaced by glutamine and Gly H10 by Ala. The three constructs differed from each other in the combination of hydrophobic residues that make up the hydrophobic core of the V$_H$-framework: in huVκ3-huV$_H$3·MocB these were derived from muV$_H$9 (Moc31), in huVκ3-V$_H$3·1 from huV$_H$1 and in huVκ3-huV$_H$3·5 from huV$_H$5.

Both hypotheses presume the existence of structural differences between V$_H$ domains derived from the muV$_H$9 germline family, and the CDR acceptor in the classical CDR graft, the huV$_H$3 consensus domain. While we do not have an experimental structure of the exact V$_H$ domains investigated in the present study, the analysis of diagnostic sequence features allows us to identify muV$_H$9 as a type III structure, and huV$_H$3 as a type II structure (Fig. 1A–D). In addition, we can compare all muV$_H$9-derived V$_H$ structures in the PDB (Berman *et al*., 2000) to all huV$_H$3-derived structures, and observe systematic structural differences between the two groups (Fig. 1E and F).

Structural comparisons of the different domain subtypes suggest that changes in the framework I kink conformation may in turn lead to clashes or under-packing in the adjacent hydrophobic core. As a result, the combination of residues that pack the hydrophobic core of the V$_H$ domain is not conserved between the subtypes. On the other side of the domain, CDR-H2 residues pack into the domain core. In particular, residue H74 (Kabat H64) is highly divergent between different V$_H$ subtypes and may not pack well with similarly divergent residues in the domain core, either leading to steric strain or to an adaptation of the CDR-H2 conformation (Fig. 3).

Superposition of the muV$_H$9-derived V$_H$ structures onto the available huV$_H$3 derived structures (many of them are themselves CDR grafts to the huV$_H$3 consensus framework) revealed subtle structural differences between the two families (Fig. 1F), outside the local differences in the FR1 region that define the subtype. Slight differences in the relative orientation of the inner and the outer β-sheet of the

domain and differences in the conformation and take-off angle of CDR-H2 between the two V_H families might have affected the antigen binding affinity. This was not the case in the Moc31 graft, as the two constructs 4D5MocA and 4D5MocB bound the antigen with similar affinity (Willuda *et al*., 1999). However, a mismatch between the conformation of the muV_H9-derived CDRs and the huV_H3-derived framework, while not sufficiently severe to alter the CDR conformation and interfere with antigen binding, may have introduced sufficient steric strain to destabilize 4D5MocA in comparison to 4D5MocB, which was designed to preserve the type III structure of the graft donor while preserving as much as possible of the human sequence and the high intrinsic stability of the huV_H3 consensus domain. If the relief of this strain in 4D5MocB were responsible for the superior stability of this construct, as stated by the second hypothesis, there would be no *intrinsic* advantage of the hybrid framework as constructed in 4D5MocB over huV_H3; rather the huV_H3 was under unusual strain with the particular set of CDRs present in the construct.

In contrast, the first hypothesis seeks the reason for the different stabilities in the domain frameworks themselves, at the source of their structural divergence: the fully buried glutamate side chain in position H6 that is a hallmark of type II frameworks is not part of a salt bridge or charge cluster, it only interacts with main-chain NH groups and the side-chain OH of Thr H143 to satisfy its hydrogen bonding requirements (Fig. 2). Normally, the burial of an uncompensated charge in the domain core is energetically highly unfavorable, and indeed the out-of-context replacement of glutamine H6 in a type III V_H domain by a glutamate will severely destabilizes the domain (Kipriyanov *et al*., 1997; de Haard *et al*., 1998; Jung *et al*., 2001). However, this glutamate is highly conserved in the germlines giving rise to subtype II domains, and type II V_H domains are overrepresented amongst the most stable V_H domains, indicating that the replacement of the Glu by an uncharged residue is evolutionally disfavored. One might think that in designing the hybrid framework 4D5MocB, we may have found a successful combination of core and subtype-determining residues, accommodating a Gln in H6 in combination with stabilizing features typical of the huV_H3 consensus. If this were the case, CDR-grafts to the hybrid framework should be more stable than grafts of the same CDRs to the huV_H3 consensus framework, independent of the structural subtype of the CDR donor.

As the data in the results section shows, thermal denaturation, midpoints of equilibrium chemical denaturation and denaturation kinetics suggest that the functional stability of the four V_H constructs can be ranked as $huV_H3 > huV_H3{\cdot}MocB > huV_H3{\cdot}5 \approx huV_H3{\cdot}1$. This ranking does not agree with the $\Delta G_{(H2O)}$-values extrapolated from a two-state fit, which would assign a very low thermodynamic stability to the scFv containing the huV_H3 domain. However, the low cooperativity of the unfolding transition of the scFv containing the huV_H3 domain is not compatible with a two-state transition, but hints at the presence of a hidden intermediate. We have thus concluded that the system is not behaving like a two-state system, and an extrapolation with very different slopes to obtain $\Delta G_{(H2O)}$ for the different mutants is not justified.

The high stability and production yield of the four constructs containing the huV_H3 consensus CDRs in comparison to both 4D5MocA and 4D5MocB, and the reduced stability of the three core-grafted constructs compared to the consensus huV_H3, all point towards the hypothesis of an improved fit between CDRs and framework. This explains the increased stability of 4D5MocB compared to 4D5MocA and of $huV\kappa3$-huV_H3 compared to the three chimeric constructs tested in this study. The data are not compatible with an increased intrinsic stability of the chimeric frameworks. This demonstrates that a CDR graft to a structurally divergent framework not only carries an increased risk of losing affinity, but may also lead to decreased stability. Furthermore, these findings of a context-dependence of the optimal framework illustrate another reason why nature has chosen to build the immune system on a set of frameworks, rather than a single one, to support the different CDRs.

Acknowledgements

A.H. and A.P. conceived the project, A.H. designed and modeled the mutants and lead the data evaluation, all authors designed experiments, A.D.M. performed the experiments, and all authors evaluated data and wrote the manuscript. We thank Hugues Bedouelle for providing the Kaleidagraph macros used to evaluate the equilibrium unfolding data.

Funding

This work was supported by the Schweizerischer Nationalfond, grant 3100AO-113720.

References

Arndt,K.M., Müller,K.M. and Plückthun,A. (1998) *Biochemistry*, **37**, 12918–12926.
Bass,S., Gu,Q.M. and Christen,A. (1996) *J. Bacteriol.*, **178**, 1154–1161.
Bentley,G.A., Boulot,G., Riottot,M.M. and Poljak,R.J. (1990) *Nature*, **348**, 254–257.
Berman,H.M., Westbrook,J., Feng,Z., Gilliland,G., Bhat,T.N., Weissig,H., Shindyalov,I.N. and Bourne,P.E. (2000) *Nucleic Acids Res.*, **28**, 235–242.
Bothmann,H. and Plückthun,A. (1998) *Nat. Biotechnol.*, **16**, 376–380.
Creighton,T.E. (1997) *Protein Structure: A Practical Approach*. 2nd edn. Oxford University Press.
de Haard,H.J.W., Kazemier,B., van der Bent,A., Oudshoorn,P., Boender,P., van Gemen,B., Arends,J.W. and Hoogenboom,H.R. (1998) *Protein Eng.*, **11**, 1267–1276.
Di Paolo,C., Willuda,J., Kubetzko,S., Lauffer,I., Tschudi,D., Waibel,R., Plückthun,A., Stahel,R.A. and Zangemeister-Wittke,U. (2003) *Clin. Cancer Res.*, **9**, 2837–2848.
Eftink,M.R. (1994) *Biophys. J.*, **66**, 482–501.
Eigenbrot,C., Randal,M., Presta,L., Carter,P. and Kossiakoff,A.A. (1993) *J. Mol. Biol.*, **229**, 969–995.
Ewert,S., Cambillau,C., Conrath,K. and Plückthun,A. (2002) *Biochemistry*, **41**, 3628–3636.
Ewert,S., Huber,T., Honegger,A. and Plückthun,A. (2003) *J. Mol. Biol.*, **325**, 531–553.
Ewert,S., Honegger,A. and Plückthun,A. (2004) *Methods*, **34**, 184–199.
Faber,C., Shan,L., Fan,Z., Guddat,L.W., Furebring,C., Ohlin,M., Borrebaeck,C.A. and Edmundson,A.B. (1998) *Immunotechnology*, **3**, 253–270.
Fellouse,F.A., Li,B., Compaan,D.M., Peden,A.A., Hymowitz,S.G. and Sidhu,S.S. (2005) *J. Mol. Biol.*, **348**, 1153–1162.
Fellouse,F.A., *et al*. (2007) *J. Mol. Biol.*, **373**, 924–940.
Gill,S.C. and von Hippel,P.H. (1989) *Anal. Biochem.*, **182**, 319–326.
Hamers-Casterman,C., Atarhouch,T., Muyldermans,S., Robinson,G., Hamers,C., Songa,E.B., Bendahman,N. and Hamers,R. (1993) *Nature*, **363**, 446–448.
Honegger,A. and Plückthun,A. (2001a) *J. Mol. Biol.*, **309**, 657–670.
Honegger,A. and Plückthun,A. (2001b) *J. Mol. Biol.*, **309**, 687–699.
Jäger,M., Gehrig,P. and Plückthun,A. (2001) *J. Mol. Biol.*, **305**, 1111–1129.

Jones,P.T., Dear,P.H., Foote,J., Neuberger,M.S. and Winter,G. (1986) *Nature*, **321**, 522–525.
Jung,S., Spinelli,S., Schimmele,B., Honegger,A., Pugliese,L., Cambillau,C. and Plückthun,A. (2001) *J. Mol. Biol.*, **309**, 701–716.
Kabat,E.A., Wu,T.T., Perry,H., Gottesmann,K. and Foeller,C. (1991) *Sequences of Proteins of Immunological Interest*. Fifth edn. NIH Publication No. 91-3242.
Kipriyanov,S.M., Moldenhauer,G., Martin,A.C., Kupriyanova,O.A. and Little,M. (1997) *Protein Eng.*, **10**, 445–453.
Knappik,A., Ge,L., Honegger,A., Pack,P., Fischer,M., Wellnhofer,G., Hoess,A., Wölle,J., Plückthun,A. and Virnekäs,B. (2000) *J. Mol. Biol.*, **296**, 57–86.
Krebber,A., Bornhauser,S., Burmester,J., Honegger,A., Willuda,J., Bosshard,H.R. and Plückthun,A. (1997) *J. Immunol. Methods*, **201**, 35–55.
Lefranc,M.P., Giudicelli,V., Kaas,Q., Duprat,E., Jabado-Michaloud,J., Scaviner,D., Ginestoux,C., Clement,O., Chaume,D. and Lefranc,G. (2005) *Nucleic Acids Res.*, **33**, D593–D597.
Lescar,J., Brynda,J., Fabry,M., Horejsi,M., Rezacova,P., Sedlacek,J. and Bentley,G.A. (2003) *Acta Crystallogr. Sect. D-Biol. Cryst.*, **59**, 955–957.
Marasco,W.A. (1995) *Immunotechnology*, **1**, 1–19.
Monsellier,E. and Bedouelle,H. (2005) *Prot. Eng. Des. Sel.*, **18**, 445–456.
Monsellier,E. and Bedouelle,H. (2006) *J. Mol. Biol.*, **362**, 580–593.
Myers,J.K., Pace,C.N. and Scholtz,J.M. (1995) *Protein Sci.*, **4**, 2138–2148.
Myklebust,A.T., Beiske,K., Pharo,A., Davies,C.D., Aamdal,S. and Fodstad,O. (1991) *Brit. J. Cancer Suppl.*, **14**, 49–53.
Pini,A., Viti,F., Santucci,A., Carnemolla,B., Zardi,L., Neri,P. and Neri,D. (1998) *J. Biol. Chem.*, **273**, 21769–21776.
Proba,K., Honegger,A. and Plückthun,A. (1997) *J. Mol. Biol.*, **265**, 161–172.
Proba,K., Wörn,A., Honegger,A. and Plückthun,A. (1998) *J. Mol. Biol.*, **275**, 245–253.
Röthlisberger,D., Pos,K.M. and Plückthun,A. (2004) *FEBS Lett.*, **564**, 340–348.
Röthlisberger,D., Honegger,A. and Plückthun,A. (2005) *J. Mol. Biol.*, **347**, 773–789.
Santoro,M.M. and Bolen,D.W. (1988) *Biochemistry*, **27**, 8063–8068.
Saul,F.A. (1994) *Res. Immunol.*, **145**, 61–66.
Saul,F.A. and Poljak,R.J. (1993) *J. Mol. Biol.*, **230**, 15–20.
Schmid,F. (2005) In Buchner,J. and Kiefhaber,T.(eds), *Protein Folding Handbook*. **Vol. 1**. WILEY-VCH Verlag GmbH & Co, pp. 22–44.
Söderlind,E., *et al*. (2000) *Nat. Biotechnol.*, **18**, 852–856.
Tanford,C. (1970) *Adv. Protein Chem.*, **24**, 1–95.
Trakhanov,S., Parkin,S., Raffai,R., Milne,R., Newhouse,Y.M., Weisgraber,K.H. and Rupp,B. (1999) *Acta Crystallogr. Sect. D-Biol. Cryst.*, **55**, 122–128.
Willuda,J., Honegger,A., Waibel,R., Schubiger,P.A., Stahel,R., Zangemeister-Wittke,U. and Plückthun,A. (1999) *Cancer Res.*, **59**, 5758–5767.
Wörn,A. and Plückthun,A. (1999) *Biochemistry*, **38**, 8739–8750.
Wörn,A., Auf der Maur,A., Escher,D., Honegger,A., Barberis,A. and Plückthun,A. (2000) *J. Biol. Chem.*, **275**, 2795–2803.

Received October 3, 2008; revised November 26, 2008; accepted November 27, 2008

Edited by Hugues Bedouelle